doi:10.1093/brain/awr130 Brain 2011: 134; 2036–2043 | 2036

BRAIN
A JOURNAL OF NEUROLOGY

Similar amyloid-β burden in posterior cortical atrophy and Alzheimer's disease

Leonardo Cruz de Souza,[1,2,3,4,5,*] Fabian Corlier,[1,2,3,4,5,*] Marie-Odile Habert,[6,7] Olga Uspenskaya,[1,2,3,4,5] Renaud Maroy,[8] Foudil Lamari,[9] Marie Chupin,[1,2,3,4] Stéphane Lehéricy,[1,2,3,4,10] Olivier Colliot,[1,2,3,4] Valérie Hahn-Barma,[1,5] Dalila Samri,[1,5] Bruno Dubois,[1,2,3,4,5] Michel Bottlaender[8] and Marie Sarazin[1,2,3,4,5]

1 Université Pierre et Marie Curie-Paris 6, Centre de Recherche de l'Institut du Cerveau et de la Moelle Épinière, UMR-S975, 47-83 bd de l'Hôpital, 75013 Paris, France
2 Inserm, U975, 47-83 bd de l'Hôpital, 75013 Paris, France
3 CNRS, UMR 7225, 47-83 bd de l'Hôpital, 75013 Paris, France
4 Institut du Cerveau et de la Moelle Épinière, ICM, 47-83 bd de l'Hôpital, 75013 Paris, France
5 Alzheimer Institute; Research and Resource Memory Centre; Centre de Référence de Démences Rares, Centre de référence maladie d'Alzheimer jeune, AP-HP, Pitié-Salpêtrière Hospital, 47-83 boulevard de l'Hôpital, 75013 Paris, France
6 AP-HP, Groupe hospitalier Pitié-Salpêtrière, Service de Médecine Nucléaire, 47-83 bd de l'Hôpital, 75013 Paris, France
7 Université Pierre et Marie Curie-Paris 6, INSERM, UMR-S 678, 47-83 bd de l'Hôpital, 75013 Paris, France
8 CEA, DSV, I2BM, Service Hospitalier Frédéric Joliot, 4, place du Général Leclerc, 91401 Orsay, France
9 Department of Metabolic Biochemistry, AP-HP, Pitié-Salpêtrière Hospital, 47-83 bd de l'Hôpital, 75013 Paris, France
10 Centre de Neuroimagerie de Recherche – CENIR and Department of Neuroradiology, Pitié-Salpêtrière Hospital, 47-83 Boulevard de l'Hôpital, 75013 Paris, France

*These authors contributed equally to this work.

Correspondence to: Dr Marie Sarazin,
Fédération des maladies du Système Nerveux,
Research and Resource Memory Centre,
Pavillon Jean Lhermitte,
Hôpital de la Salpêtrière,
47 Boulevard de l'Hôpital,
75013 Paris,
France
E-mail: marie.sarazin@psl.aphp.fr

While the clinical presentation of posterior cortical atrophy is clearly distinct from typical Alzheimer's disease, neuropathological studies have suggested that most patients with posterior cortical atrophy have Alzheimer's disease with an atypical visual presentation. We analysed *in vivo* pathophysiological markers of Alzheimer's disease such as cerebrospinal fluid biomarkers and positron emission tomography imaging with ^{11}C-labelled Pittsburgh compound-B in posterior cortical atrophy to determine whether biochemical profile and fibrillar amyloid-β burden topography are associated with the clinical presentation. Nine patients with posterior cortical atrophy and nine with typical Alzheimer's disease individually matched for age, duration and severity of the disease and 10 cognitively normal age-matched controls were included. ^{11}C-labelled Pittsburgh compound-B images were analysed both using volumes of interest and on a voxel-wise basis using statistical parametric mapping, taking into account the individual regional cortical atrophy. Cerebrospinal fluid biomarkers did not differ between posterior cortical atrophy and patients with Alzheimer's disease. Compared with normal controls, both posterior cortical atrophy and Alzheimer's disease

Received February 16, 2011. Revised April 7, 2011. Accepted April 18, 2011

groups showed increased ^{11}C-labelled Pittsburgh compound-B uptake. No significant difference was found in regional or global ^{11}C-labelled Pittsburgh compound-B binding between posterior cortical atrophy and Alzheimer's disease groups with both volumes of interest and voxel-wise basis using statistical parametric mapping methods. Our findings demonstrate that cerebrospinal fluid biomarkers and positron emission tomography imaging with ^{11}C-labelled Pittsburgh compound-B may be useful in identifying an atypical visual form of Alzheimer's disease. The similar topography of fibrillar amyloid-β deposition between typical Alzheimer's disease and posterior cortical atrophy groups suggests that, although amyloid-β accumulation plays a critical role in the pathogenesis of Alzheimer's disease, other factors such as neurofibrillary tangles may contribute to the different clinical features observed in posterior cortical atrophy.

Keywords: Alzheimer's disease; posterior cortical atrophy; Pittsburgh compound-B

Abbreviations: ^{11}C-PIB = ^{11}C-labelled Pittsburgh compound-B; PCA = posterior cortical atrophy

Introduction

Posterior cortical atrophy (PCA) can be defined as an atypical form of Alzheimer's disease, as shown by neuropathological studies (Renner *et al*., 2004; Tang-Wai *et al*., 2004; Alladi *et al*., 2007). However, the clinical presentation of PCA is clearly distinct from typical Alzheimer's disease (Dubois *et al*., 2010). In PCA, disease onset is characterized by visual disturbances, followed by an impairment of visuospatial skills, while episodic memory is relatively spared (McMonagle *et al*., 2006). Neuroimaging shows atrophy and hypoperfusion/hypometabolism that predominates in the parieto-occipital cortex regions (Lehmann *et al*., 2009), with a relative sparing of the temporal regions (Aharon-Peretz *et al*., 1999; Nestor *et al*., 2003). This clinical presentation contrasts with typical Alzheimer's disease, which is characterized by an early episodic memory deficit associated with prominent medial temporal lobe atrophy.

Pathophysiological markers can help identify the underlying aetiology of PCA (Dubois *et al*., 2010). CSF biomarker levels are considered to reflect Alzheimer pathology and can be useful in isolating patients with an atypical Alzheimer's disease phenotype (Baumann *et al*., 2010; de Souza *et al*., 2011). ^{11}C-labelled Pittsburgh compound-B (^{11}C-PIB)-PET scanning measures the fibrillar amyloid-β deposition (Ikonomovic *et al*., 2008). Only two cases of PCA have been published with details of ^{11}C-PIB binding showing a high amyloid-β burden in the occipital cortex (Ng *et al*., 2007; Migliaccio *et al*., 2009), which is not the most affected region in Alzheimer's disease (Kemppainen *et al*., 2006). Better characterization of CSF and PET amyloid deposition profiles in patients with PCA would improve diagnosis and facilitate inclusion in clinical trials of Alzheimer's disease-modifying drugs.

We aimed to analyse both CSF biomarkers and ^{11}C-PIB-PET profiles in subjects with PCA. Because PCA and Alzheimer's disease are likely to have the same underlying neuropathological process, we hypothesize that the two groups would present similar CSF and PIB binding patterns. Therefore, we studied the topography of amyloid deposition in PCA compared with Alzheimer's disease to examine whether the different clinical presentations of PCA and typical Alzheimer's disease were associated with a distinct distribution and burden of fibrillar amyloid-β deposition.

Materials and methods

Subjects

Nine patients with PCA were enrolled on the basis of following diagnostic criteria (McMonagle *et al*., 2006; Alladi *et al*., 2007): (i) insidious onset and gradual progression of cognitive impairment beginning with visual complaints; (ii) presentation with visuospatial deficits with intact primary visual function; (iii) features suggestive of Bálint's syndrome (optic ataxia, ocular apraxia and simultagnosia) associated or not with Gerstmann's (acalculia, agraphia, left–right disorientation and finger agnosia) syndrome; (iv) proportionally less episodic memory impairment; (v) relatively preserved insight; and (vi) glucose hypometabolism on ^{18}F-fluorodeoxyglucose-PET examination and prominent cortical atrophy in the posterior cortical region on MRI. A complete Bálint's syndrome was observed in seven of nine patients with PCA, while incomplete Bálint's syndrome was present in two of nine subjects (isolated simultagnosia for one patient, and simultagnosia with oculomotor apraxia for the other). In addition, complete Gerstmann's syndrome was observed in three of nine patients with PCA; incomplete Gerstmann's syndrome was present in six of nine patients. Ideomotor apraxia, acalculia, agraphia and environmental disorientation were observed for eight of nine patients, visual agnosia, hemineglect and finger agnosia were present in seven of nine patients and dressing apraxia in five of nine patients with PCA (refer to Supplementary Table 1 for details).

Nine typical patients with Alzheimer's disease were individually matched with subjects with PCA for age, duration of disease and disease severity assessed by the Clinical Dementia Rating scale score. Individual matching was used to avoid a selection bias caused by these parameters. All subjects with Alzheimer's disease were selected according to the New Research Criteria (Dubois *et al*., 2007, 2010), which include (i) progressive episodic memory impairment, characterized by a low free recall not normalized with cueing; (ii) CSF Alzheimer's disease profile, defined as score below 0.8 for the ratio of amyloid-β_{42}:tau, calculated with the formula amyloid-β_{42}/[240 + (1.18 × T-tau)] (Visser *et al*., 2009); and (iii) clinical dementia rating scale $\geqslant$0.5.

Ten healthy elderly controls were recruited for the study according to the following criteria: (i) Mini-Mental State Examination score $\geqslant$28/30 and clinical dementia rating scale = 0; (ii) no history of neurological or psychiatric disorders; and (iii) no memory complaint or cognitive deficit.

Subjects were not included in the study if they presented any of the following criteria: (i) systemic illnesses that could interfere with

cognitive functioning; (ii) extrapyramidal signs or neurological history suggestive of Parkinson's disease with dementia, progressive supranuclear palsy, corticobasal degeneration or dementia with Lewy bodies; (iii) vascular lesions on MRI or neurological history suggestive of vascular dementia; or (iv) depression assessed with a score >20 on the Montgomery-Asberg Depression Rating Scale (MADRS; Montgomery and Asberg, 1979).

Blood samples were drawn to characterize APOE genotypes. The controls underwent the same procedures as did the patients with PCA and Alzheimer's disease, except for lumbar puncture, which was not proposed due to ethical reasons.

The study was conducted by the French National Institute of Health and Medical Research (INSERM; ANR-07-LVIE-002-01) and was approved by the Ethics Committee of Pitié-Salpêtrière Hospital. All subjects provided written informed consent before participating.

Clinical, functional and cognitive assessment

All subjects (healthy controls, Alzheimer's disease and PCA) underwent a clinical and neuropsychological examination that included the Mini-Mental State Examination (Folstein *et al*., 1975), the clinical dementia rating scale (Morris, 1993) and tests for assessing verbal episodic memory, executive functions, working memory, gesture praxis and visuoconstructive function. In addition, subjects with PCA underwent a specific 'posterior neuropsychological battery' assessing hemineglect, spatial disorientation, body schema distortion, Bálint's and Gerstmann's syndromes (Kas *et al*., 2011).

Cerebrospinal fluid biomarker analysis

CSF samples obtained by lumbar puncture were processed with the same procedures described previously (de Souza *et al*., 2011) to obtain CSF levels of total tau (T-tau), phosphorylated tau at threonine 181 (P-Tau) and amyloid-β peptide 1-42 (amyloid-β_{42}) by using enzyme-linked immunosorbent assay kits (Innogenetics), according to the manufacturer's instructions. All operators were blind to clinical information.

Magentic resonance imaging procedure

In each participant, the imaging data were collected using a 3 T Siemens 32-channel TRIO TIM system using 12-channel head coil for signal reception. The MRI examination included a 3D T_1-weighted volumetric magnetization-prepared rapid-gradient echo sequence with repetition time = 2300 ms, echo time = 3.43 ms, inversion time = 900, 256 × 256 matrix, axial field of view and slice thickness 1 mm. This sequence provided a high grey/white matter contrast-to-noise ratio and allowed for excellent segmentation and accurate coregistration with the PET images.

Positron emission tomography imaging procedure

Data acquisition

PET examinations were performed with a High Resolution Research Tomograph (HRRT, Siemens Medical Solution), the camera with the highest available spatial resolution for brain imaging. The spatial resolution for the HRRT scanner was 2.5 mm with an absolute sensitivity of 6% for a point source in the centre of the field of view. The HRRT had an axial field of view of 25 cm and a transaxial field of view of 31.2 cm. It allowed the reconstruction of 207 slices of 1.1 mm thickness. Subjects were positioned in the tomograph with the head maintained using an individually moulded head holder. A 6-min brain transmission scan was performed before injection of each radioligand using a ^{137}Cs point source to correct the emission scan for tissue attenuations. ^{11}C-PIB (mean 364 ± 47 MBq) was injected intravenously, and PET acquisitions lasted 90 min. Twenty-five images were reconstructed with a scan duration starting from 1 min and increasing up to 10 min during the experiment. All images were reconstructed with an accelerated list-mode, ordinary Poisson ordered-subset expectation maximization (OP-OSEM) algorithm, including an experimental stationary model of the scanner spatial resolution that allowed for a lowering or the statistical noise at the voxel level in the reconstructed images without degrading spatial resolution (Sureau *et al*., 2008). This method improved quantitative accuracy by reducing the partial volume effects.

Volume of interest analysis

Parametric images were created using Brainvisa software (http://brainvisa.info). The cerebellum was used as a reference region in the analysis because this region has been found to be spared from amyloid plaque accumulation (Joachim *et al*., 1989). Standard uptake value parametric images were constructed on late images over 50–70 min because this time schedule has been shown to be more accurate (Lopresti *et al*., 2005). Standard uptake value-ratio parametric images were constructed by dividing each pixel by the corresponding value obtained in the cerebellum. The parametric images were coregistered individually with the corresponding 3D magnetic resonance T_1 images using the Brainvisa software.

All volumes of interests were delineated on the individual MRI scans for each subject as described below.

Segmentation: the T_1 weighted images were segmented with the Brainvisa software. The cortical and sub-cortical grey matter, white matter and cerebellum were delineated using histogram analysis, threshold methods and morphological operators. A parcellation of the cortex into 76 structures was then performed in three steps: (i) non-linear registration of the subject's segmented cortex on the Montreal Neurological Institute grey matter template and application of the inverse transformation to the Automated Anatomic Labeling atlas; (ii) masking of this resampled volume of labels by the segmented cortex structure and filling of the cortex mask using a Voronoi diagram; and (iii) minimization of the gyri interface distance to the nearest sulci bottoms extracted using a regional deformable model. The amygdala and hippocampi were automatically segmented in each individual using the T_1-weighted MRIs and the SACHA software (Chupin *et al*., 2009).

Automated Anatomic Labeling segmentation provided values of ^{11}C-PIB fixation in 76 anatomical regions. The volumes of interest were defined separately for the left and right hemispheres and were pooled into greater anatomical regions based on anatomical relationships to obtain a mean ^{11}C-PIB-standard uptake value-ratio for each region, as described in the legend of Fig. 1. As a measure of global amyloid burden, we calculated a ^{11}C-PIB global index, representing the subject's mean standard uptake value-ratio in all the defined regions (Fig. 1).

Voxel-based analysis and preprocessing

MRI data were spatially normalized using SPM5 (Wellcome Trust Centre for Neuroimaging) and the Montreal Neurological Institute template, and then segmented to isolate the grey matter partition. In an effort to avoid a bias group effect resulting from spatial normalization, the procedure included the creation of a customized template

Table 1 Demographic and clinical data of studied groups

	PCA	Alzheimer's disease	Controls
Number of subjects	9	9	10
Female/male	7/2*	6/3	2/8
Age (years)	62.9 ± 3.5 (59.5–69)	62.0 ± 2.7 (58–65.5)	65.8 ± 6.8 (59–75.5)
Education (years)	12.6 ± 2.6[§] (9–15)	14.7 ± 1.0 (12–15)	13.3 ± 2.35 (9–15)
Disease duration (years)	2.1 ± 1.8 (1–6)	2.6 ± 1.3 (1–5)	–
Mini-Mental State Examination	17.1 ± 5.9** (9–27)	19.4 ± 3.8** (15–25)	29.2 ± 1.0 (27–30)
Clinical dementia rating scale	0.5, $n = 3$ 1, $n = 3$ 2, $n = 3$	0.5, $n = 4$ 1, $n = 3$ 2, $n = 2$	0 for all subjects
Amyloid-β42 (pg/ml)	303 ± 73 (209–400)	236 ± 92 (125–386)	NA
T-tau (pg/ml)	511 ± 290 (319–1183)	540 ± 266 (175–1106)	NA
P-tau (pg/ml)	76 ± 34 (45–143)	86 ± 28 (29–123)	NA
Ratio of amyloid-β_{42}:Tau	0.4 ± 0.1 (0.2–0.6)	0.3 ± 0.1 (0.1–0.4)	NA

Data are presented as mean ± standard deviation (min–max).
[§]$P < 0.05$ versus Alzheimer's disease subjects; *$P < 0.05$ versus controls; **$P < 0.001$ versus controls. NA = not applicable.

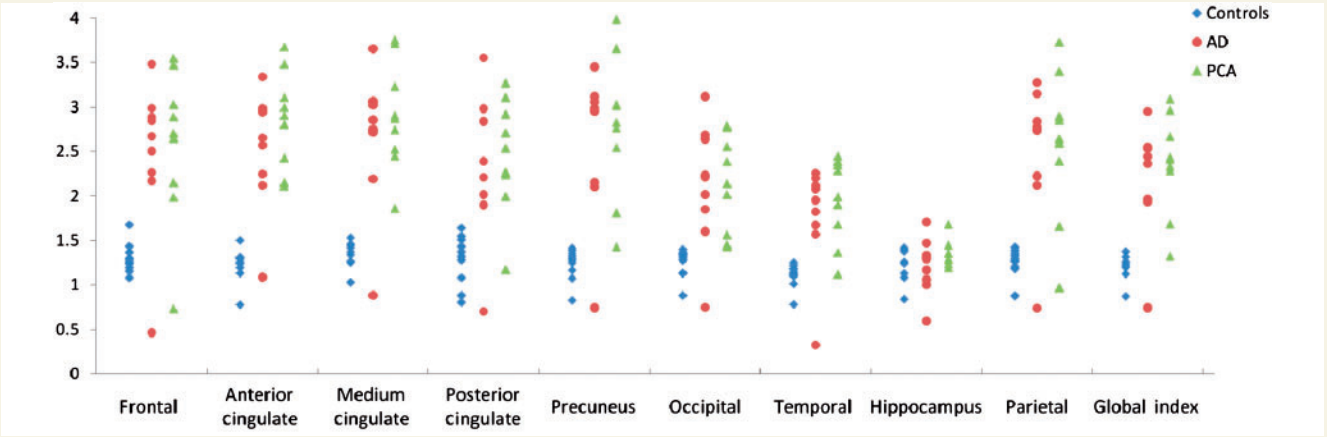

Figure 1 Scatter plots showing ^{11}C-PIB-standard uptake value-ratio in anatomical regions across groups [healthy controls (diamonds), Alzheimer's disease (circles), PCA (triangles)]. Anatomical regions were pooled from volumes of interests provided by Automated Anatomic Labeling segmentation and were defined as the following: (i) frontal cortex by grouping orbitofrontal, polar prefrontal and dorsolateral cortex; (ii) anterior cingulate; (iii) medium cingulated; (iv) posterior cingulate; (v) precuneus; (vi) occipital cortex by grouping calcarine cortex, occipital cortex and cuneus; (vii) temporal cortex by grouping anterior and lateral temporal cortex; (viii) hippocampus; and (ix) parietal cortex by grouping inferior and superior parietal cortex and the parietotemporal junction. The ^{11}C-PIB global index representing the subject's mean standard uptake value-ratio in the regions is described above. AD = Alzheimer's disease.

of the grey matter using the MRI data from the whole combined patient and control samples ($n = 28$). Grey matter data were then renormalized using this customized template. A whole grey matter mask was obtained by thresholding the grey matter density average image above a value of 0.2, corresponding to a 20% chance that the voxel belongs to the grey matter (Chetelat *et al.*, 2008).

Four ^{11}C-PIB PET frames of 5 min each from 50 to 70 min post-injection were realigned with SPM5, and a mean volume was calculated from these four frames for each subject. The mean ^{11}C-PIB-PET volumes were then coregistered to their corresponding MRI and spatially normalized, applying the transformation parameters obtained from MRI normalization. A partial volume effect was minimized by (i) the reconstruction algorithm described above (Sureau *et al.*, 2008); and (ii) by multiplying each normalized mean ^{11}C-PIB image by its corresponding whole grey matter mask. Each partial volume effect corrected ^{11}C-PIB image was then divided by its corresponding mean cerebellum PIB standard uptake value, resulting in parametric standard uptake value-ratio images. The mean cerebellum activity was obtained from a custom mask drawn on the Montreal Neurological Institute single subject MRI provided by SPM. The PIB-standard uptake value-ratio images were then smoothed (full width at half maximum = 10 mm).

Statistical analysis

The clinical data, CSF biomarker levels, mean ^{11}C-PIB-standard uptake value-ratio in each volume of interest and global PIB index group were compared between the PCA, Alzheimer's disease and healthy controls groups using a non-parametric Kruskal–Wallis one-way analysis of variance. The homogeneity of variances was assessed with the Levene and

Brown-Forsythe tests. The Bonferroni correction for multiple comparisons was applied. The chi-square test was used to compare gender ratios. An alpha (significance) level of 0.05 was chosen. All statistical analyses were performed using PASW Statistics 18 (© SPSS Inc). For SPM analyses, the statistical threshold was set at $P < 0.001$, and false discovery rate corrected.

Results

Subjects characteristics

Clinical characteristics of subjects with PCA, Alzheimer's disease and healthy controls are presented in Table 1. The Mini-Mental State Examination score did not differ between the PCA and Alzheimer's disease groups, whereas both groups significantly differed from the healthy control group ($P < 0.001$).

Cerebrospinal fluid biomarker analysis

CSF biomarker levels in the PCA and Alzheimer's disease groups are presented in Table 1. No statistical differences were found between the PCA and Alzheimer's disease groups for amyloid-β_{42}, T-tau, P-tau levels or for the amyloid-β_{42}:Tau ratio. In accordance with the inclusion criteria, individual analysis showed that all patients with Alzheimer's disease had abnormal ratios of amyloid-β_{42}:Tau. All patients with PCA had a CSF Alzheimer's disease profile, and the highest amyloid-β_{42}:Tau ratio observed in this group was 0.6.

Pittsburgh compound-B: region of interest analysis

The Alzheimer's disease and PCA groups showed higher global ^{11}C-PIB index and higher ^{11}C-PIB uptake values in all regions of interest when compared with normal controls, except for the hippocampal region (Table 2). The mean PIB indices were identical in the PCA and Alzheimer's disease groups, and no significant differences in regional PIB uptake were detected between both groups in any region of interest.

Individual analysis showed that one patient with Alzheimer's disease had no significant ^{11}C-PIB uptake regardless of the region studied. This 65-year-old female had a typical clinical history of Alzheimer's disease, with onset of memory deficit 2 years before inclusion in the study. The Mini-Mental State Examination was 19/30, and the clinical dementia rating scale was 0.5. The CSF analysis revealed a biological profile of Alzheimer's disease with a low amyloid-β_{42} level (125 pg/ml) and an unusually high increase of T-tau (1016 pg/ml) and P-tau (123 pg/ml) levels. The EEG was normal. The clinical follow-up (18 months) was in agreement with the diagnosis. There was no argument for a frontotemporal dementia on clinical and neuroimaging investigations (MRI and fluorodeoxyglucose-PET). A 60-year-old female with PCA (Mini-Mental State Examination = 14; clinical dementia rating scale = 1) had a global ^{11}C-PIB index overlapping with the highest score measured in controls, although regional analysis showed a high ^{11}C-PIB uptake in the anterior and medium cingulate and occipital cortices. The CSF biomarkers showed a low amyloid-β_{42} level (246 pg/ml) with normal T-tau (336 pg/ml) and high P-tau levels (67 pg/ml) and an abnormal ratio of amyloid-β_{42}:Tau (0.38).

Pittsburgh compound-B: voxel-wise comparisons

Compared with normal controls, patients with Alzheimer's disease showed significant symmetrical ^{11}C-PIB binding throughout the frontal and parietal cortices, precuneus and cingulate regions (Fig. 2A), and patients with PCA showed diffuse and symmetric ^{11}C-PIB binding in the frontal, parietal, temporal cortices, cingulate and precuneus (Fig. 2B). Direct SPM comparison of the two patient groups showed no voxel in which PIB uptake was greater in one or another group, even at a lower threshold of $P < 0.001$ uncorrected for multiple comparisons.

Discussion

In our study, we used CSF biomarkers and ^{11}C-PIB-PET amyloid binding, which are markers of Alzheimer's disease lesions, to

Table 2 Neocortical mean (±SD) ^{11}C-PIB standard uptake value-ratio in anatomical regions

	Healthy controls ($n = 10$)	Alzheimer's disease ($n = 9$)	PCA ($n = 9$)
Frontal	1.30 (±0.17)	2.66 (±0.97)*	2.57 (±0.86)* NS
Anterior cingulate	1.23 (±0.19)	2.69 (±0.73)*	2.85 (±0.55)* NS
Medium cingulate	1.32 (±0.17)	2.79 (±0.86)*	2.89 (±0.61)* NS
Posterior cingulate	1.29 (±0.29)	2.53 (±0.84)*	2.47 (±0.64)* NS
Precuneus	1.24 (±0.18)	2.79 (±0.88)*	2.79 (±0.80)* NS
Occipital	1.26 (±0.16)	2.23 (±0.72)*	2.12 (±0.54)* NS
Temporal	1.11 (±0.13)	1.88 (±0.63)*	1.95 (±0.48)* NS
Hippocampus	1.24 (±0.20)	1.22 (±0.31)	1.36 (±0.16) NS
Parietal	1.26 (±0.15)	2.66 (±0.83)*	2.57 (±0.84)* NS
Global index	1.22 (±0.15)	2.37 (±0.71)*	2.35 (±0.57)* NS

*Significant ($P < 0.001$) when compared with healthy group; NS = non-significant ($P > 0.05$) when compared with Alzheimer's disease group.

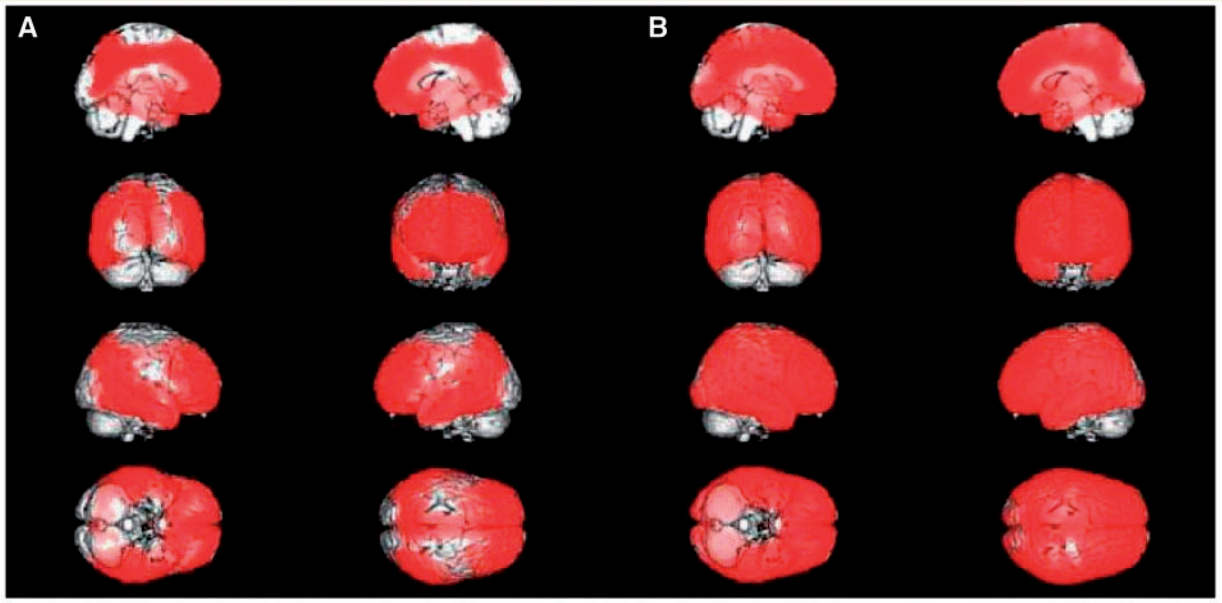

Figure 2 Topography of ^{11}C-PIB standard uptake value-ratio in the grey matter of nine patients with Alzheimer's disease (**A**) and in the grey matter of nine patients with PCA (**B**) compared with 10 normal healthy controls. In both the Alzheimer's disease and PCA group, increased ^{11}C-PIB standard uptake value-ratio involves widespread areas in the frontal, parietal, temporal and posterior cingulate cortices (significance threshold set at $P < 0.001$ corrected for false discovery rate).

investigate *in vivo* the neuropathological process of patients with PCA. The positivity of both pathophysiological markers indicated the presence of Alzheimer pathology in favour of the diagnosis of atypical Alzheimer's disease. In addition, using two different methods of analysis, no difference in the load and topography of amyloid-β deposition assessed by ^{11}C-PIB-PET was observed between the PCA and Alzheimer's disease groups, suggesting that amyloidosis cannot explain the differences in the Alzheimer's disease/PCA clinical presentations.

PCA is a rare disease, and we included a small number of patients in our analysis. To avoid selection bias, we individually matched each patient with PCA with a patient with Alzheimer's disease for age, duration of disease and disease severity. Patients with PCA had a similar profile of CSF biomarkers as compared with patients with Alzheimer's disease. Neuropathological studies demonstrated that the combination of amyloid-β_{42}, T-tau and P-tau levels in ante-mortem CSF predicted the presence of Alzheimer's disease-associated pathological changes with high accuracy, supporting the idea that these CSF changes are a surrogate marker for the diagnosis of Alzheimer's disease (Bian *et al*., 2008; Tapiola *et al*., 2009). Previous studies have also suggested that CSF biomarkers may be useful to identify *in vivo* atypical focal forms of Alzheimer's disease such as PCA (Baumann *et al*., 2010; de Souza *et al*., 2011), although these observations were not supported by ^{11}C-PIB-PET or autopsy data. The present study extends these results by providing molecular imaging support.

PIB binding is highly selective for insoluble fibrillar amyloid-β deposits. Direct correlation of *in vivo* ^{11}C-PIB retention with quantitative analyses of amyloid-β plaques was demonstrated in a post-mortem study (Ikonomovic *et al*., 2008) and supports the validity of ^{11}C-PIB-PET imaging as a method for the *in vivo* evaluation of amyloid-β plaque burden. High PIB uptake was observed in 80–100% of patients with Alzheimer's disease (Rowe *et al*., 2007; Rabinovici *et al*., 2010). In the current study, the CSF diagnosis of Alzheimer's disease in the PCA group was in accordance with the ^{11}C-PIB-PET imaging showing higher ^{11}C-PIB binding in subjects with PCA as compared with controls, and similar PIB binding as compared with patients with Alzheimer's disease. One subject with PCA had a PIB index that overlapped with the control values, although the subject had a biological CSF diagnosis of Alzheimer's disease. Interestingly, regional analysis showed high PIB binding in the anterior and median cingulate regions and a milder increase in the occipital cortex. One patient with Alzheimer's disease did not show evidence of elevated ^{11}C-PIB binding, despite having the typical Alzheimer's disease clinical presentation and CSF biomarkers profile. Failure of ^{11}C-PIB to detect amyloid-β pathology in Alzheimer's disease has already been reported (Rabinovici *et al*., 2010.), even in one patient with a pathological confirmation of Alzheimer's disease (Cairns *et al*., 2009).

Taken together, CSF biomarkers and ^{11}C-PIB-PET provided arguments to establish *in vivo* the diagnosis of atypical Alzheimer's disease in patients with PCA. Clinicopathological investigations have demonstrated that Alzheimer's pathology is the most frequent cause of PCA, accounting for 80–100% of all cases (Renner *et al*., 2004; Tang-Wai *et al*., 2004; Alladi *et al*., 2007). Other diagnoses such as Lewy-body dementia, corticobasal degeneration and Creutzfeldt–Jakob (Renner *et al*., 2004) are rare. The fact that all patients with PCA in our study had no parkinsonism and had a disease onset characterized by visual disturbance could explain the homogeneity of our data. Future

studies including autopsy diagnoses are needed to confirm our findings.

An unresolved challenge remains how to explain the differences in clinical presentation between PCA and Alzheimer's disease despite a similar burden of amyloidosis. PCA is characterized by early higher order visual deficits (Benson *et al*., 1988). Patients develop features of Bálint's syndrome (ocular apraxia, optic ataxia and simultanagnosia), Gerstmann's syndrome (acalculia, agraphia, finger agnosia, and left–right disorientation), visual agnosia and transcortical sensory aphasia, whereas episodic memory is preserved or only mildly impaired. Structural and functional neuroimaging has also demonstrated parieto-occipital atrophy and hypoperfusion/hypometabolism in a focal pattern that is clearly different from Alzheimer's disease (Nestor *et al*., 2003; Schmidtke *et al*., 2005; Lehmann *et al*., 2009; Kas *et al*., 2011).

One way to understand this singular clinical presentation of PCA is to assess the amyloid topography between both diseases in order to evaluate whether amyloidosis is related to the atypical visual form of Alzheimer's disease. Descriptive data about ^{11}C-PIB binding in PCA are scarce. In two PCA cases, ^{11}C-PIB uptake was increased in the occipital (Ng *et al*., 2007) and right calcarine cortices (Kambe *et al*., 2010). We did not confirm higher ^{11}C-PIB uptake in the posterior cortical regions with our larger sample of nine patients with PCA who fulfilled strict inclusion criteria. No significant differences in ^{11}C-PIB burden and distribution between patients with PCA and Alzheimer's disease were observed either using a region of interest method or a voxel-based approach. The absence of a relationship between the clinical symptoms of Alzheimer's disease and amyloid deposition is supported by several arguments: (i) PIB binding in Alzheimer's disease was not correlated with the severity of dementia assessed by the Mini-Mental State Examination (Engler *et al*., 2006) or the clinical dementia rating scale (Jack *et al*., 2009); (ii) amyloid deposition remains stable during Alzheimer's disease follow-up (2 years) despite further decreases in cognitive function and cortical glucose metabolism (Engler *et al*., 2006); (iii) the differences in clinical presentation between the early and late onset Alzheimer's disease groups was not related to amyloid burden (Rabinovici *et al*., 2010); and (iv) the progression of the amyloid deposition in the human brain (from neocortical regions to cerebellum) does not correspond to the clinical progression of symptoms in Alzheimer's disease (Thal *et al*., 2002).

The similar topography of fibrillar amyloid-β deposition between typical Alzheimer's disease and PCA groups provides support for the model in which amyloidosis plays a critical role in Alzheimer's disease pathogenesis. Other factors such as neurofibrillary tangles may contribute to the atypical visual clinical presentation (Jack *et al*., 2002; Csernansky *et al*., 2004). Indeed, autopsies have reported a greater density of neurofibrillary tangles in PCA than in Alzheimer's disease; these are most notable in the primary visual and visual associative cortex. Autopsies have also found a smaller density of tangles in the hippocampus and subiculum, with a similar density of senile plaques in cortical areas (Tang-Wai *et al*., 2004).

To conclude, we hypothesize that amyloid-β pathology in PCA occurs at an early phase of the disease, similar to the timing seen in typical Alzheimer's disease, and that the clinical presentation of PCA may result from an interaction with tau-pathology. Because PCA is similar to Alzheimer's disease in terms of amyloid-β pathology but differs in its tau-pathology progression, PCA provides a model to study *in vivo* the interaction between amyloid and tau pathology, an interaction that is still poorly understood.

^{11}C-PIB-PET and CSF biomarkers have the potential to identify candidate patients with PCA who may benefit from specific therapeutic strategies targeting amyloid-β metabolism. The therapeutic windows during which treatment should be initiated should be discussed with regard to the present data, which provide support for early therapeutic interventions.

Acknowledgements

We are greatly indebted to the chemical/radiopharmaceutical and nursing staff of Service Hospitalier Frédéric Joliot for the synthesis of the ^{11}C-PIB and patient management, respectively.

Funding

French agence Nationale de la Recherche (ANR) under reference ANR-07-LVIE-002-01, French Fondation Nationale de Gerontologie and MEDIAPART; 'Fondation pour la Recherche Médicale' (to L.C.dS.). During the two last years, Dr L.C.dS. has collaborated with the pharmaceutical company Lundbeck; European Federation of Neurological Societies (EFNS to Dr O.U.). Mr F.C., Dr M.-O.H., Dr O.U., Dr R.M., Dr F.L., Dr O.C., Ms D.S. and Mrs V.H.-B. report no conflict of interest. During the two last years, Dr M.C. and Pr S.L. have collaborated with the pharmaceutical company EISAI. During the two last years, Pr B.D. has collaborated with the pharmaceutical companies EISAI, Novartis, Roche, Bristol-Mayer-Squib, Servier. During the two last years, Dr M.B. has collaborated with the pharmaceutical company IPSEN-BEAUFOUR. During the two last years, Dr M.S. has collaborated with the pharmaceutical companies EISAI, Novartis, Pfizer, Lundbeck.

Supplementary material

Supplementary material is available at *Brain* online.

References

Aharon-Peretz J, Israel O, Goldsher D, Peretz A. Posterior cortical atrophy variants of Alzheimer's disease. Dement Geriatr Cogn Disord 1999; 10: 483–7.

Alladi S, Xuereb J, Bak T, Nestor P, Knibb J, Patterson K, et al. Focal cortical presentations of Alzheimer's disease. Brain 2007; 130: 2636–45.

Baumann TP, Duyar H, Sollberger M, Kuhle J, Regeniter A, Gomez-Mancilla B, et al. CSF-tau and CSF-Abeta(1-42) in posterior cortical atrophy. Dement Geriatr Cogn Disord 2010; 29: 530–3.

Benson DF, Davis RJ, Snyder BD. Posterior cortical atrophy. Arch Neurol 1988; 45: 789–93.

Bian H, Van Swieten JC, Leight S, Massimo L, Wood E, Forman M, et al. CSF biomarkers in frontotemporal lobar degeneration with known pathology. Neurology 2008; 70: 1827–35.

Cairns NJ, Ikonomovic MD, Benzinger T, Storandt M, Fagan AM, Shah AR, et al. Absence of Pittsburgh compound B detection of cerebral amyloid beta in a patient with clinical, cognitive, and cerebrospinal fluid markers of Alzheimer disease: a case report. Arch Neurol 2009; 66: 1557–62.

Chetelat G, Desgranges B, Landeau B, Mezenge F, Poline JB, de la Sayette V, et al. Direct voxel-based comparison between grey matter hypometabolism and atrophy in Alzheimer's disease. Brain 2008; 131: 60–71.

Chupin M, Hammers A, Liu R, Colliot O, Burdett J, Bardinet E, et al. Automatic segmentation of the hippocampus and the amygdala driven by hybrid constraints: method and validation. Neuroimage 2009; 46: 749–61.

Csernansky JG, Hamstra J, Wang L, McKeel D, Price JL, Gado M, et al. Correlations between antemortem hippocampal volume and postmortem neuropathology in AD subjects. Alzheimer Dis Assoc Disord 2004; 18: 190–5.

de Souza LC, Lamari F, Belliard S, Jardel C, Houillier C, De Paz R, et al. Cerebrospinal fluid biomarkers in the differential diagnosis of Alzheimer's disease from other cortical dementias. J Neurol Neurosurg Psychiatry 2011; 82: 240–6.

Dubois B, Feldman HH, Jacova C, Cummings JL, Dekosky ST, Barberger-Gateau P, et al. Revising the definition of Alzheimer's disease: a new lexicon. Lancet Neurol 2010; 9: 1118–27.

Dubois B, Feldman HH, Jacova C, Dekosky ST, Barberger-Gateau P, Cummings J, et al. Research criteria for the diagnosis of Alzheimer's disease: revising the NINCDS-ADRDA criteria. Lancet Neurol 2007; 6: 734–46.

Engler H, Forsberg A, Almkvist O, Blomquist G, Larsson E, Savitcheva I, et al. Two-year follow-up of amyloid deposition in patients with Alzheimer's disease. Brain 2006; 129: 2856–66.

Folstein MF, Folstein SE, McHugh PR. 'Mini-mental state'. A practical method for grading the cognitive state of patients for the clinician. J Psychiatr Res 1975; 12: 189–98.

Ikonomovic MD, Klunk WE, Abrahamson EE, Mathis CA, Price JC, Tsopelas ND, et al. Post-mortem correlates of in vivo PiB-PET amyloid imaging in a typical case of Alzheimer's disease. Brain 2008; 131: 1630–45.

Jack CR Jr, Dickson DW, Parisi JE, Xu YC, Cha RH, O'Brien PC, et al. Antemortem MRI findings correlate with hippocampal neuropathology in typical aging and dementia. Neurology 2002; 58: 750–7.

Jack CR Jr, Lowe VJ, Weigand SD, Wiste HJ, Senjem ML, Knopman DS, et al. Serial PIB and MRI in normal, mild cognitive impairment and Alzheimer's disease: implications for sequence of pathological events in Alzheimer's disease. Brain 2009; 132: 1355–65.

Joachim CL, Morris JH, Selkoe DJ. Diffuse senile plaques occur commonly in the cerebellum in Alzheimer's disease. Am J Pathol 1989; 135: 309–19.

Kambe T, Motoi Y, Ishii K, Hattori N. Posterior cortical atrophy with ^{11}C Pittsburgh compound B accumulation in the primary visual cortex. J Neurol 2010; 257: 469–71.

Kas A, de Souza LC, Samri D, Bartolomeo P, Lacomblez L, Kalafat M, et al. Neural correlates of cognitive impairment in posterior cortical atrophy. Brain 2011; 134: 1464–78.

Kemppainen NM, Aalto S, Wilson IA, Nagren K, Helin S, Bruck A, et al. Voxel-based analysis of PET amyloid ligand ^{11}CPIB uptake in Alzheimer disease. Neurology 2006; 67: 1575–80.

Lehmann M, Crutch SJ, Ridgway GR, Ridha BH, Barnes J, Warrington EK, et al. Cortical thickness and voxel-based morphometry in posterior cortical atrophy and typical Alzheimer's disease. Neurobiol Aging 2009; doi:10.1016/j.neurobiolaging.2009.08.017.

Lopresti BJ, Klunk WE, Mathis CA, Hoge JA, Ziolko SK, Lu X, et al. Simplified quantification of Pittsburgh Compound B amyloid imaging PET studies: a comparative analysis. J Nucl Med 2005; 46: 1959–72.

McMonagle P, Deering F, Berliner Y, Kertesz A. The cognitive profile of posterior cortical atrophy. Neurology 2006; 66: 331–8.

Migliaccio R, Agosta F, Rascovsky K, Karydas A, Bonasera S, Rabinovici GD, et al. Clinical syndromes associated with posterior atrophy: early age at onset AD spectrum. Neurology 2009; 73: 1571–8.

Montgomery SA, Asberg M. A new depression scale designed to be sensitive to change. Br J Psychiatry 1979; 134: 382–9.

Morris JC. The Clinical Dementia Rating (CDR): current version and scoring rules. Neurology 1993; 43: 2412–4.

Nestor PJ, Caine D, Fryer TD, Clarke J, Hodges JR. The topography of metabolic deficits in posterior cortical atrophy (the visual variant of Alzheimer's disease) with FDG-PET. J Neurol Neurosurg Psychiatry 2003; 74: 1521–9.

Ng SY, Villemagne VL, Masters CL, Rowe CC. Evaluating atypical dementia syndromes using positron emission tomography with carbon ^{11} labelled Pittsburgh Compound B. Arch Neurol 2007; 64: 1140–4.

Rabinovici GD, Furst AJ, Alkalay A, Racine CA, O'Neil JP, Janabi M, et al. Increased metabolic vulnerability in early-onset Alzheimer's disease is not related to amyloid burden. Brain 2010; 133: 512–28.

Renner JA, Burns JM, Hou CE, McKeel DW Jr, Storandt M, Morris JC. Progressive posterior cortical dysfunction: a clinicopathologic series. Neurology 2004; 63: 1175–80.

Rowe CC, Ng S, Ackermann U, Gong SJ, Pike K, Savage G, et al. Imaging beta-amyloid burden in aging and dementia. Neurology 2007; 68: 1718–25.

Schmidtke K, Hull M, Talazko J. Posterior cortical atrophy: variant of Alzheimer's disease? A case series with PET findings. J Neurol 2005; 252: 27–35.

Sureau FC, Reader AJ, Comtat C, Leroy C, Ribeiro MJ, Buvat I, et al. Impact of image-space resolution modeling for studies with the high-resolution research tomograph. J Nucl Med 2008; 49: 1000–8.

Tang-Wai DF, Graff-Radford NR, Boeve BF, Dickson DW, Parisi JE, Crook R, et al. Clinical, genetic, and neuropathologic characteristics of posterior cortical atrophy. Neurology 2004; 63: 1168–74.

Tapiola T, Alafuzoff I, Herukka SK, Parkkinen L, Hartikainen P, Soininen H, et al. Cerebrospinal fluid {beta}-amyloid 42 and tau proteins as biomarkers of Alzheimer-type pathologic changes in the brain. Arch Neurol 2009; 66: 382–9.

Thal DR, Rub U, Orantes M, Braak H. Phases of A beta-deposition in the human brain and its relevance for the development of AD. Neurology 2002; 58: 1791–800.

Visser PJ, Verhey F, Knol DL, Scheltens P, Wahlund LO, Freund-Levi Y, et al. Prevalence and prognostic value of CSF markers of Alzheimer's disease pathology in patients with subjective cognitive impairment or mild cognitive impairment in the DESCRIPA study: a prospective cohort study. Lancet Neurol 2009; 8: 619–27.